Arabian Journal for Science and Engineering (2022) 47:7053–7067
https://doi.org/10.1007/s13369-021-06302-2

RESEARCH ARTICLE-CHEMISTRY

Mannich Base as an Efficient Corrosion Inhibitor of AA6061 in 0.5 M HCl: Electrochemical, Surface Morphological and Theoretical Investigations

K. Maithili[1] · Prakasha Shetty[1] · P. Preethi Kumari[1] · Sneha Kagatikar[1]

Received: 19 April 2021 / Accepted: 12 October 2021 / Published online: 14 November 2021

Abstract
The inhibition action of a Mannich base, N-(1- morpholinobenzyl) semicarbazide (MBS), was examined on AA6061 corrosion in 0.5 M HCl solution at varied temperatures (303 to 323 K). The testing was performed by potentiodynamic polarization (PDP) and electrochemical impedance spectroscopy (EIS) techniques. The inhibition performance of MBS was improved with an increment in its concentration (0.01–2.56 mM) and temperature rise (303 to 323 K). MBS showed a mixed inhibitor behavior at all concentrations and temperatures range studied. MBS displayed the highest inhibition efficiency of 98% at 2.56 mM and 323 K. Inhibitor followed mixed adsorption on the alloy surface and obeyed the Langmuir isotherm model. The results obtained from the EIS were in good agreement with that of the PDP results. An appropriate mechanism was proposed for the corrosion inhibition of AA6061. Inhibitor molecules adsorption on alloy surface was confirmed by surface morphology testing by a scanning electron microscope (SEM) and atomic force microscope (AFM). Theoretical studies using density-functional theory (DFT) confirmed the experimental results.

Keywords AA6061 · Mannich base · Electrochemical techniques · Corrosion control · Adsorption

1 Introduction

The commercial aluminum alloys belong to the AA6xxx series are mainly composed of Mg and Si as the major alloying elements. These Al alloys have widespread applications in aircraft, automobile, and marine industries due to their high strength-to-weight ratio, suitable extrusion, rolling capabilities, and good corrosion resistance [1, 2]. Al alloys have shown good corrosion resistance properties because they could form a stable oxide barrier of Al_2O_3 on the surface when it comes in contact with a neutral solution or atmosphere [3]. However, the pickling agent like the hydrochloric acid solution used during their surface treatment can destroy the protective oxide layer, leading to heavy metal loss. Hence, the excessive dissolution of metal in such cases can be avoided by adding a suitable inhibitor to the pickling medium. Although different combating corrosion methods are available, adding an appropriate inhibitor to the corrosive medium is the easiest and most cost-effective method [4, 5].

In acidic conditions, the most commonly used inhibitors of corrosion are organic compounds. The most effective inhibitors are the organic compounds containing heteroatoms, electron-donating functional groups, and π bonds [6–8]. There is a need for extensive investigation on the corrosion of AA6061 and subsequent development of an efficient corrosion inhibitor for AA6061 that can be easily used and exhibit excellent inhibition performance. Mannich bases are the beta ketone-carrying compounds that display potent pharmaceutical activities [9]. Some researchers have used Mannich bases as efficient corrosion inhibitors for mild steel [10–14]. However, they have not been investigated for their corrosion inhibition activity toward Al alloys. In this work, we aim to exploit a Mannich base, N-(1- morpholinobenzyl) semicarbazide (MBS), as an inhibitor for AA6061 in the presence of 0.5 hydrochloric acid medium at various concentrations of inhibitor and different temperatures. The corrosion inhibitor MBS used in the present work can be easily synthesized. MBS evinced inhibition efficiency as high as 98% at 2.56 mM concentration and 323 K.

✉ Prakasha Shetty
prakash.shetty@manipal.edu

[1] Department of Chemistry, Manipal Institute of Technology, Manipal Academy of Higher Education, Manipal, Karnataka 576104, India

2 Experimental Procedures

2.1 Material

AA6061 alloy was the material employed in the experimental work. Its elemental composition in wt. % is Mg (0.82), Si (0.51), Mn (0.15), Fe (0.68), Cu (0.16), Cr (0.04), and Al (97.64).

2.2 AA6061 Specimen

A cylindrical specimen of AA6061 was cut from the rod of the alloy sample. The specimen was embedded in the epoxy resin by cold setting, leaving 1 cm^2 of the exposed cut surface. The exposed surface was abraded with emery papers of various grades (200 to 1500). Besides, the abraded specimen was mirror polished on a disk polisher using levigated alumina as an abrasive material. It was then washed in distilled water, rinsed in acetone, and finally dried.

2.3 Medium

A solution of 0.5 M HCl was prepared using distilled water with an appropriate dilution of 37% analytical grade hydrochloric acid. It was standardized by the volumetric method.

2.4 Preparation of Inhibitor

The proposed inhibitor, MBS, was prepared by following the reported procedure [15]. Semicarbazide hydrochloride (1.11 g, 10 mM) was dissolved in a minimum amount of distilled water and added 20 ml ethanol. The solution was then neutralized with the dropwise addition of concentrated NH_3. To this, morpholine (0.9 ml, 10 mM) was added dropwise with stirring. Then, benzaldehyde (1 ml, 10 mM) was also added dropwise with further stirring. After five min. of continuous stirring, a colorless solid precipitated was filtered, dried, and recrystallized with ethanol. Finally, it was characterized by FTIR and NMR spectroscopy. IR spectra were recorded in the frequency range 4000–400 cm^{-1} using a Shimadzu FTIR (8400S) spectrophotometer and KBr. ^{1}H-NMR spectra of the sample were measured in DMSO-d_6 using the NMR spectrophotometer (Bruker 400 MHz). The structural formula of MBS is shown in Fig. 1.

2.5 Electrochemical Studies

Electrochemical testing was performed with a CH Instruments (CH600D-series, the US model) embedded with beta software and a three-electrode cell system comprised of a calomel electrode (as reference electrode), a working electrode of AA6061, and an auxiliary electrode of platinum.

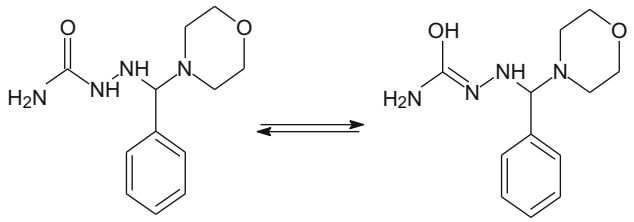

Fig. 1 The structural formula of MBS (Keto and Enol form)

Experiments were performed in a 0.5 M HCl as the corrosive medium and freshly abraded AA6061 specimen with an exposed surface area of 1cm^2 at different temperatures (303, 313, and 323 K). A calibrated digital thermostat was used to maintain the temperature accurately within ± 0.5 K. Freshly prepared solutions and freshly abraded specimens were used in each experiment. Each measurement with three trials was taken to ensure the reliability and reproducibility of the data.

The AA6061 working electrode was initially allowed to stand for about 30 min in a 0.5 M HCl to obtain a steady open circuit potential (OCP) value. Later on, potentiodynamic polarization was carried out by subjecting the system to the potential from − 250 mV cathodic to + 250 mV anodic with 1 mV/s scan rate. Tafel plots were recorded, and PDP parameters like E_{corr} (corrosion potential), i_{corr} (corrosion current density), anodic (β_a), and cathodic (β_c) Tafel slopes were noted. EIS measurements were taken by applying a 10 mV amplitude AC signal in the 10 kHz–0.01 Hz frequency range. Impedance data processing was performed using the Nyquist plots.

2.6 Surface Analysis of AA6061 Specimen

The surface morphology of the AA6061 specimen immersed in the 0.5 M hydrochloric acid medium without and with 2.56 mM MBS for 3 h. were recorded using an analytical scanning electron microscope (JEOL JSM-6380L model). An atomic force microscope (IB342-Innova model) was employed to record the roughness of the corroded and inhibited surface of the AA6061 specimen.

2.7 Ultraviolet–Visible (UV/Vis) Spectroscopy

UV–Vis spectra of 0.5 M HCl with 0.01 mM of MBS were initially recorded using an 1800 Shimadzu UV–Visible spectrophotometer. Later the absorption spectra of the 0.5 M HCl solution containing 0.01 mM MBS after immersion of a test coupon of AA6061 for 1 h were recorded.

2.8 Quantum Chemical Studies

Density-functional theory (DFT) simulation studies were performed using the B3LYP functions of Schrodinger's mate-

rial science suite with a 6-31G + + basis set. 2D and 3D molecular builders recorded the MBS molecule's optimized structure, highest occupied molecular orbital (HOMO), and lowest unoccupied molecular orbital (LUMO). Various parameters like global hardness and softness, ionization potential, electronegativity, and electron transfer fraction were calculated.

3 Results and Discussion

3.1 Characterization of MBS

Colorless crystalline solid (80%); $C_{12}H_{18}N_4O_2$; m.p. 216 ± 1 °C; IR (KBr) [cm^{-1}]: 3288 (NH str.), 3028 (Ar. CH str.), 1643 (C=N str.), 1600 (C=O str.), 1141 (C-O str.). ^{1}H NMR (400 MHz, DMSO-d_6) (δppm): 10.94 (1H, –N=C–OH), 7.83 (2H, -NH_2), 6.7 (1H, -CH), 6.32–7.72 (5H, Ar. H), 6.23 (1H, NH), 3.74 (4H, -O-CH_2), 2.5 (4H, –N–CH_2).

3.2 Corrosion Inhibition of AA6061

3.2.1 PDP Studies

The Tafel plots for AA6061 alloy specimen immersed in 0.5 M HCl without and with varying concentrations of MBS at 313 K are presented in Fig. 2a.

The PDP parameters such as E_{corr}, i_{corr}, β_c, and β_a were obtained from these plots. The corrosion rate was computed as per the equation,

$$\mathrm{CR}\left(\mathrm{mmy}^{-1}\right) = \frac{3270 \times M \times i_{\mathrm{corr}}}{d \times Z} \tag{1}$$

In this relation, i_{corr} refers to corrosion current density (mA/cm^2), d indicates the density (g/cm^3), M is the atomic mass of corroding material, Z is the number of electrons transferred [16].

The inhibition efficiency (IE) of MBS was computed from the relation,

$$\mathrm{IE}(\%) = \frac{i_{\mathrm{corr}} - i_{\mathrm{corr}(inh)}}{i_{\mathrm{corr}}} \times 100 \tag{2}$$

where i_{corr} and $i_{corr(inh)}$ indicate the corrosion current in the blank and inhibited solutions, respectively [16].

The PDP results in Table 1 indicate that the alloy's corrosion current and corrosion rate in the inhibited solution have decreased with rising MBS concentration, increasing IE. However, IE of MBS was found to decrease with a rise in temperature up to 0.64 mM concentration of MBS. However, from 2 mM MBS, IE increases with temperature (Fig. 2b). It may be due to the physisorption of MBS at its lower concentrations and chemisorption at higher concentrations with a rise in temperature [17]. The maximum *IE* of 96.42% was observed for 2.56 mM MBS at 323 K.

In the Tafel plot (Fig. 2a), the anodic curve corresponds to metal oxidation, whereas the cathodic curve corresponds to the hydrogen evolution reaction. There are two inflections in the anodic curve, which may be due to the kinetic barrier effect. This may arise either due to pore formation in the passivation layer or due to its breakage. Consequently, a considerable change in the Tafel anodic slope (β_a) was observed due to the existence of passivation in the potential range of − 0.7 V to − 0.6 V [18]. It is clear from Table 1 that there is no considerable variation in the cathodic Tafel slope (β_c) in the inhibited medium. This indicates that the addition of MBS to the acid medium increased the energy barrier of the cathodic reaction, leading to a considerable reduction in hydrogen evolution reaction. Besides, the presence of MBS did not alter the inhibition mechanism [19, 20].

It is evident from Table 1 that the corrosion potential observed in the presence of MBS has not altered significantly. As per Li et al. [21], if the shift in E_{corr} value in the inhibited solution is more than ± 85 mV than in the blank solution, the inhibitor employed belongs to either cathodic or anodic type. In this work, the increase in E_{corr} value obtained for MBS is less than 85 mV, suggesting the mixed inhibitor behavior of MBS and hence controls both the anode and cathode reactions.

3.2.2 EIS studies

The Nyquist plot for AA6061 corrosion in blank and inhabited solutions at 313 K is depicted in Fig. 3a. Under other temperatures tested, similar plots have been obtained. As per Fig. 3a, impedance plots obtained were semicircular, revealing that corrosion is a process regulated by charge transfer [22]. The literature has reported similar impedance plots for inhibiting AA6061 corrosion in HCl medium [23]. Figure 3a shows a depressed capacitive loop in the higher frequency region and an inductive loop in the lower frequency region. This behavior is known as frequency dispersion which arises due to the alloy surface's inhomogeneities [24].

As per the literature [25], an exponential factor acts as a deviation parameter from the impedance function's ideal behavior. Thus, one capacitor in the equivalence circuit could be replaced by CPE (constant phase element). CPE is an element dependant on the frequency and is surface-related.

The impedance function of CPE is given by,

$$Z_{\mathrm{CPE}} = (A(i\omega)^n)^{-1} \tag{3}$$

A is the proportionality coefficient related to both the surface and electroactive species. The n value ($-1 \leq n \leq 1$)

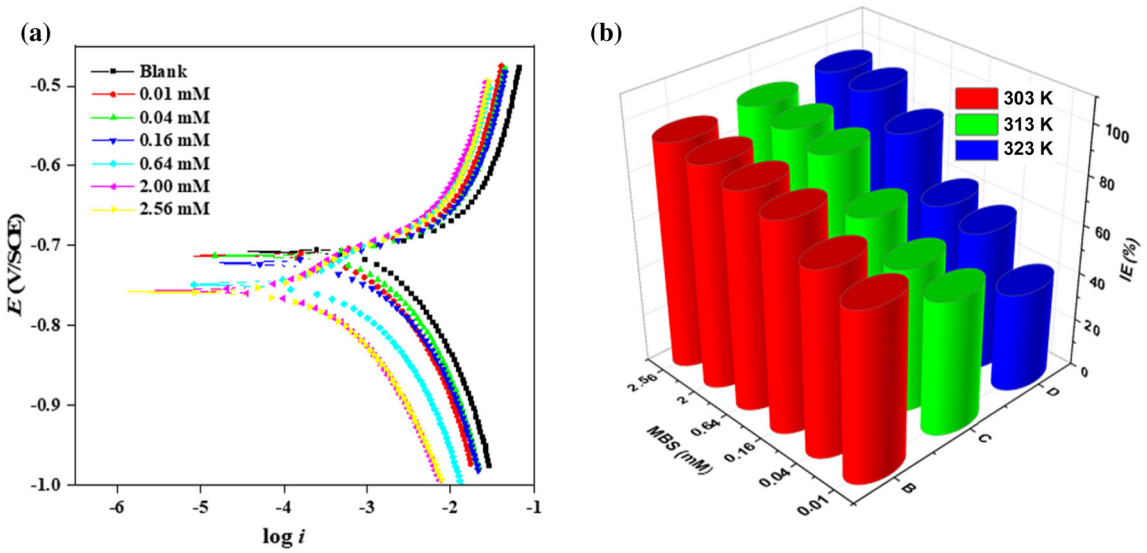

Fig. 2 **a** Tafel plot for AA6061 corrosion in blank and inhibited solution at 313 K and **b** variation of IE (%) with temperature

Table 1 PDP results for AA6061 in the blank and inhibited medium at different temperatures

Temp. (K)	Conc. Of MBS (mM)	E_{corr} (V vs SCE)	I_{corr} (mA/cm^2)	CR (mmy^{-1})	β_a (V dec^{-1})	β_c (V dec^{-1})	IE (%)
303	0.0	− 0.698	2.365	25.86	6.058	6.789	–
	0.01	− 0.726	0.7008	7.663	9.124	6.766	70.36
	0.04	− 0.727	0.5544	6.063	9.251	6.971	76.56
	0.16	− 0.761	0.3174	3.472	22.846	6.279	86.58
	0.64	− 0.748	0.2394	2.619	16.362	7.490	89.88
	2.00	− 0.762	0.1822	1.992	22.014	7.253	92.29
	2.56	− 0.750	0.1473	1.610	18.524	7.436	93.77
313	0.0	− 0.713	3.782	41.35	5.442	6.040	–
	0.01	− 0.719	1.669	18.25	6.033	6.371	55.86
	0.04	− 0.718	1.514	16.56	5.584	6.289	59.97
	0.16	− 0.733	1.050	11.48	7.472	6.464	72.23
	0.64	− 0.763	0.3986	4.359	17.376	6.302	89.46
	2.00	− 0.756	0.2835	3.101	13.217	7.226	92.50
	2.56	− 0.758	0.1931	2.112	14.276	7.074	94.89
323	0.0	− 0.727	14.68	160.6	4.653	4.007	–
	0.01	− 0.734	8.606	94.11	4.911	4.759	41.38
	0.04	− 0.733	6.112	66.85	4.774	4.472	58.36
	0.16	− 0.737	5.565	60.86	4.814	4.060	62.09
	0.64	− 0.738	2.303	25.18	5.479	6.445	84.30
	2.00	− 0.748	0.7391	8.082	7.538	7.051	94.96
	2.56	− 0.748	0.5247	5.738	7.855	7.305	96.42

depends on surface morphology, and ω indicates the angular frequency. At the same time, i is an imaginary number [26].

C_{dl} (double-layer capacitance) value was computed using the relationship:

$$C_{dl} = \frac{1}{2\pi R_P f_{\max}} \tag{4}$$

where. $f_{\max}$ indicates the Nyquist plot's frequency at which the imaginary part of the impedance is maximum [27].

An oxide layer formation and charge transfer could cause the high-frequency region's capacitive loop during the corrosion process. The oxide film formed could be considered as the capacitor's parallel circuit due to dielectric properties and resistors due to the oxide film's ionic conductance [28].

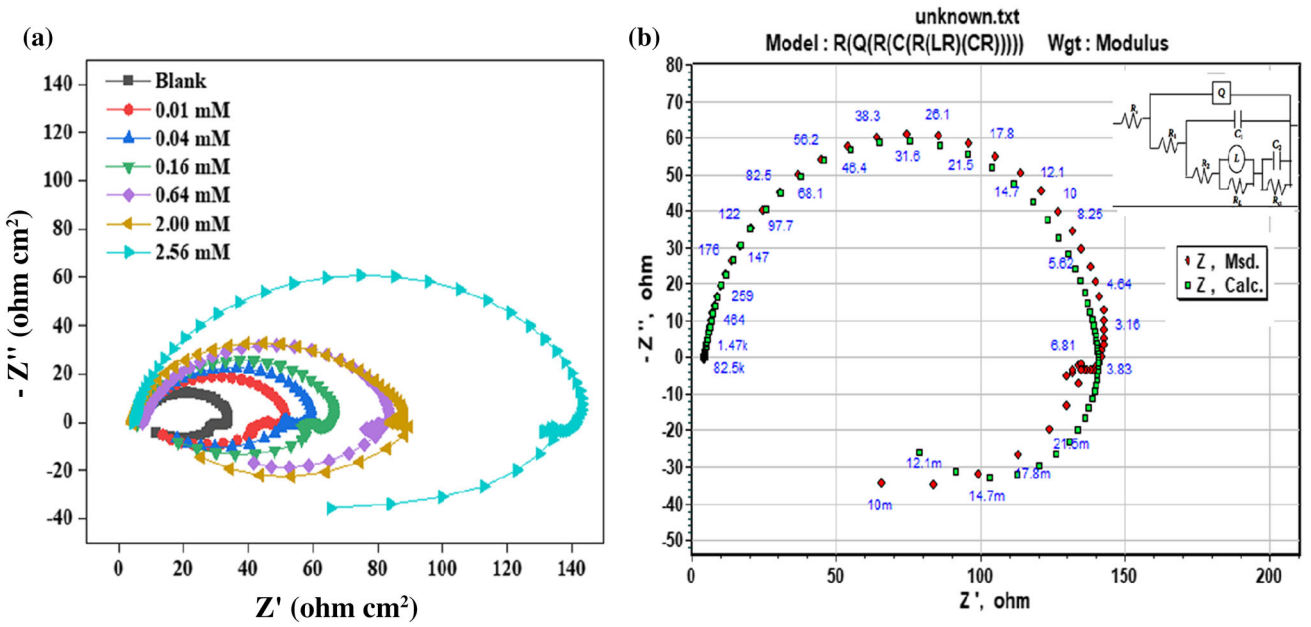

Fig. 3 **a** Nyquist plot for AA6061 corrosion in blank and inhibited solution at 313 K, and **b** stimulated plot and the fitment circuit of equivalence

As per Brett [29], interfacial reactions lead to a capacitive loop. Interfacial reactions involve the formation of the Al^{+} ions at the Al/oxide interface. They subsequently get diffused through the oxide/electrolyte interface and finally oxidized to Al^{3+} ions along with the formation of OH^{-} or O^{2-} ions. The three processes can be represented in one loop due to loop overlap or dominance of any one process. The inductive loop in the low-frequency region could be caused by bulk or surface relaxation processes occurring at oxide layer [30]. Hence, this could be related to the adsorption of charged inhibitor species onto the oxide layer. It may also contribute to an increase in the inductive loop's diameter with the increase in inhibitor concentration, which indicates an increase in resistance toward the corrosive attack on the alloy surface due to the adsorption of MBS [31].

A suitable equivalent circuit comprising nine elements was obtained using Zwimp software (version 3.21) to find the best match for the impedance plots. Figure 3b represents the stimulating fitment plot. The corresponding equivalent circuit depicted in Fig. 3b comprises elements such as R_{ct} (charge transfer resistance), R_s (solution resistance), Q (constant phase element), R_L and L (inductive components), C_1 and C_2 (capacitors), and R_1, R_2, R_L,R_{ct} (resistors). In this case, Q is parallel to C_1 and C_2, whereas R_L is parallel to L. For the circuit fitment, R_p (polarization resistance) and C_{dl} (double-layer capacitance) are computed from Eg. (4) and (5), respectively.

$$R_p = R_1 + R_2 + R_L + R_{ct} \tag{5}$$

$$C_{dl} = C_1 + C_2 \tag{6}$$

Since the R_p value varies inversely as the i_{corr} value, IE of MBS can be computed from the equation:

$$\mathrm{IE}(\%) = \frac{R_{p(\mathrm{inh})} - R_p}{R_{p(\mathrm{inh})}} \times 100 \tag{7}$$

$R_{p(\mathrm{inh})}$ indicates the inhibited solution's polarization resistance while Rp is in the blank solution [25].

Inhibition efficiency values computed from the impedance data are listed in Table 2. We can infer from Table 2 that the R_p values increased as the MBS concentration increases. But the R_p values decreased with rising in temperature up to 0.64 mM MBS. From 2.00 mM MBS concentration, the R_p value increased with temperature, indicating a decrease in the value of i_{corr}. The increase in R_p value with MBS concentration is mainly due to increased resistance to electron flow by the adsorbed inhibitor film on the alloy surface. The C_{dl} value decreased with a rise in MBS concentration because there was an increase in the double-layer thickness at the alloy/solution interface [32]. Apart from this, the decrease in C_{dl} values may also be due to replacing water molecules on alloy surfaces with MBS molecules [31].

3.2.3 Effect of Temperature

The influence of temperature on the adsorption behavior of inhibitors helps to obtain thermodynamic parameters such as E_a (activation energy), ΔH_a (enthalpy of activation), and ΔS_a (entropy of activation). It is evident from Table 1 that up to 0.64 mM MBS, there is a decrease in IE with rising temperature, which could be due to the shorter time lag between the

Table 2 EIS results for AA6061 in the blank and inhibited medium at different temperatures

Temp. (K)	Conc. of MBS (mM)	R_p (Ω cm^2)	C_{dl} (μFcm^{-2})	IE (%)
303	Blank	53.8	118	–
	0.01	143	34.3	62.46
	0.04	161	29.7	66.66
	0.16	212	17.7	74.62
	0.64	297	10.2	81.87
	2.00	361	9.63	85.11
	2.56	400	6.07	86.56
313	Blank	34.1	210	–
	0.01	70.5	101	51.63
	0.04	94.6	65.9	63.94
	0.16	132	44.9	74.23
	0.64	283	17.7	87.94
	2.00	480	9.23	92.89
	2.56	748	5.71	95.32
323	Blank	12.8	772	–
	0.01	21.7	2980	40.99
	0.04	29.8	2200	57.01
	0.16	34.0	1310	62.40
	0.64	104	197	87.74
	2.00	999	8.15	98.71
	2.56	1340	5.83	98.92

adsorption and desorption of MBS molecules from the alloy surface. This indicates the physisorption of MBS occurring on the alloy surface up to 0.64 mM [33]. However, there is an increase in IE with temperature from 2 mM MBS, which shows stronger chemisorption of MBS.

The energy of activation (E_a) can be obtained by using Arrhenius law as per the equation:

$$\ln(CR) = B - \frac{E_a}{RT} \tag{8}$$

In this equation, B is the Arrhenius constant, R is the universal gas constant (8.314 JK^{-1}mol^{-1}), and T is the absolute temperature [34].

Figure 4a represents the Arrhenius plot for AA6061 in 0.5 M HCl without and with MBS. This plot [ln (CR) vs. $1/T$] shows a straight line with a slope equal to ($-E_a/R$). The E_a values for both blank and inhibited solutions were obtained from the slope.

ΔH_a and ΔS_a values have computed by using the transition state theory equation as given below:

$$CR = \frac{RT}{Nh} \exp\left(\frac{\Delta S_a}{R}\right) \exp\left(\frac{\Delta H_a}{RT}\right) \tag{9}$$

where h is the Planck's constant and N is the Avogadro's number [35].

ln(CR/T) against $1/T$ graph for AA6061 in the blank and inhibited solutions at varying temperatures is depicted in Fig. 4b. The obtained straight-line graph gives the slope equal to -$\Delta H_a/R$ and the intercept equal to ln(R/Nh) + $\Delta S_a/R$. In Table 3, activation parameters for AA6061 in blank and inhibited solutions at different temperatures have been listed.

The E_a value (Table 3) in the blank solution was less than the corresponding values for inhibited solution. The higher E_a value in the inhibited solution showed a greater energy barrier for corrosion, blocking the transfer of charges on the alloy surface and controls corrosion [36]. It reveals the physical adsorption of MBS (up to 0.64 mM) on the alloy surface. The lower E_a values at 2.00 and 2.56 mM MBS in the inhibited medium compared to the blank solution indicate MBS's chemisorption on the alloy surface [37]. The positive ΔH_a values indicate the endothermic nature of the dissolution of alloy in an acid medium. The positive value of ΔS_a suggests that as the reactants progress to the activated complex state on the metal/solution interface, an increase in disordering occurs, which drives the adsorption process [38].

3.2.4 Adsorption Isotherm

Generally, organic inhibitors control the corrosion of metals in an aggressive medium through the adsorption process. In such cases, it is important to known the type of adsorption isotherm model followed. For this, the degree of surface cov-

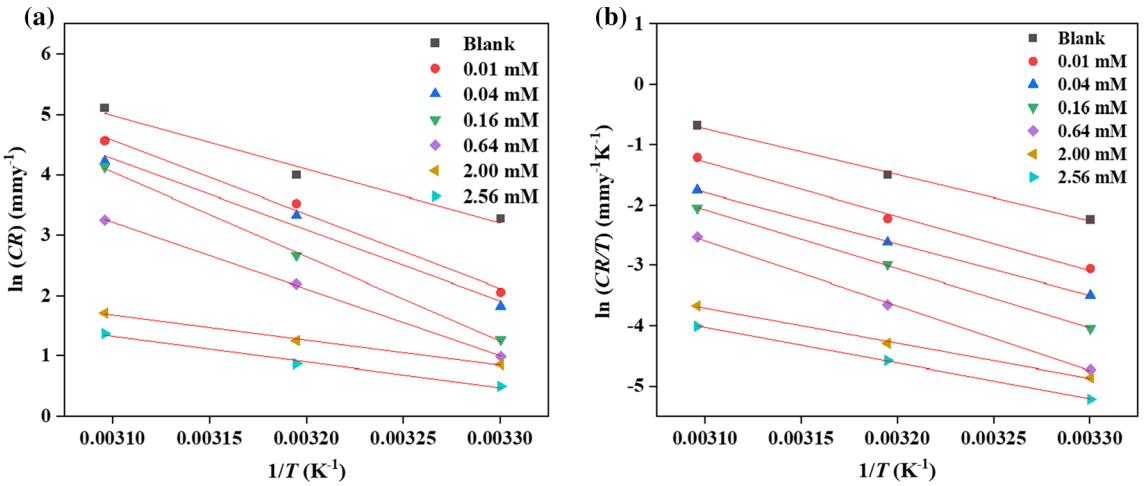

Fig. 4 **a** Arrhenius plot and **b** plot of ln(*CR*/*T*) Vs. 1/*T* for AA6061 at different temperatures in blank and inhibited medium

Table 3 Activation parameters for AA6061 in the blank and inhibited medium

Conc. of MBS (mM)	E_a (kJmol^{-1})	ΔH_a (kJmol^{-1})	ΔS_a (Jmol^{-1}K^{-1})
0	73.89	71.29	16.17
0.01	94.50	90.05	80.00
0.04	97.45	94.85	82.52
0.16	116.27	113.67	139.85
0.64	91.51	88.91	54.81
2.00	50.73	48.13	− 80.02
2.56	51.36	48.76	− 81.01

erage (θ) values of inhibitor at varying concentrations must be known, and it can be calculated using the equation:

$$\theta = \frac{\text{IE}}{100} \tag{10}$$

The values of θ obtained were fitted with adsorption isotherm models such as Langmuir, Temkin, and Freundlich. The best fit was obtained for isotherm adsorption of Langmuir. According to the Langmuir adsorption model, θ can be related to the concentration of MBS (C_{inh}) as per the equation:

$$\frac{C_{\text{inh}}}{\theta} = \frac{1}{K_{\text{ads}}} + C_{\text{inh}} \tag{11}$$

In this relation, K_{ads} indicates the equilibrium constant for adsorption (Lmol^{-1}), and $C_{(inh)}$ indicates MBS concentration [39]. Figure 5a depicts the Langmuir adsorption isotherm plot (C_{inh}/θ Vs. C_{inh}) for MBS adsorption on AA6061 in 0.5 M HCl at varied temperatures. A straight-line graph was obtained having an intercept value equal to $1/K_{\text{ads}}$. The slope and linear regression coefficient obtained are close to unity, which indicates that the Langmuir isotherm model is followed [40]. The value of $\Delta G^{\circ}_{\text{ads}}$ (standard free energy of adsorption) was determined from the known K_{ads} (Equilibrium constant for adsorption) value using the equation:

$$K_{\text{ads}} = \frac{1}{55.5} e\left(\frac{-\Delta G^{\circ}_{\text{ads}}}{RT}\right) \tag{12}$$

The solution's water concentration is 55.5 mol/L, T indicates the temperature, and R refers to the universal gas constant [41].

The $\Delta G^{\circ}_{\text{ads}}$ value is related to the $\Delta H^{\circ}_{\text{ads}}$ (enthalpy of adsorption), and $\Delta S^{\circ}_{\text{ads}}$ (entropy of adsorption) values as per the relation:

$$\Delta G^{0}_{\text{ads}} = \Delta H^{0}_{\text{ads}} - T\Delta S^{0}_{\text{ads}} \tag{13}$$

By the plot, $\Delta G^{\circ}_{\text{ads}}$ vs. T, a straight-line graph (Fig. 5b) obtained with slope and regression coefficient values closer to unity (Table 4) indicates a good correlation between the different thermodynamic parameters. The $\Delta S^{\circ}_{\text{ads}}$ and $\Delta H^{\circ}_{\text{ads}}$ values are obtained, respectively, from the slope and intercept value. All the thermodynamic results obtained from Fig. 5 are tabulated in Table 4.

In general, the value of $\Delta G^{\circ}_{\text{ads}}$ less than or equal to −20 kJmol^{-1} indicates the interaction of the charged inhibitor species with the metal surface, resulting in physisorption. On the other hand, the value of $\Delta G^{\circ}_{\text{ads}}$ equal to or greater than −40 kJmol^{-1} indicates the charge transfer from inhibitor to the metal surface, resulting in chemisorption [42]. From Table 4, it is evident that $\Delta G^{\circ}_{\text{ads}}$ value for MBS adsorption on the alloy surface at different temperatures is greater than −20 kJmol^{-1}, and it is also approaching 40 kJmol^{-1}. Thus, MBS's followed mixed adsorption, i.e., both physisorption and chemisorption. The negative sign of

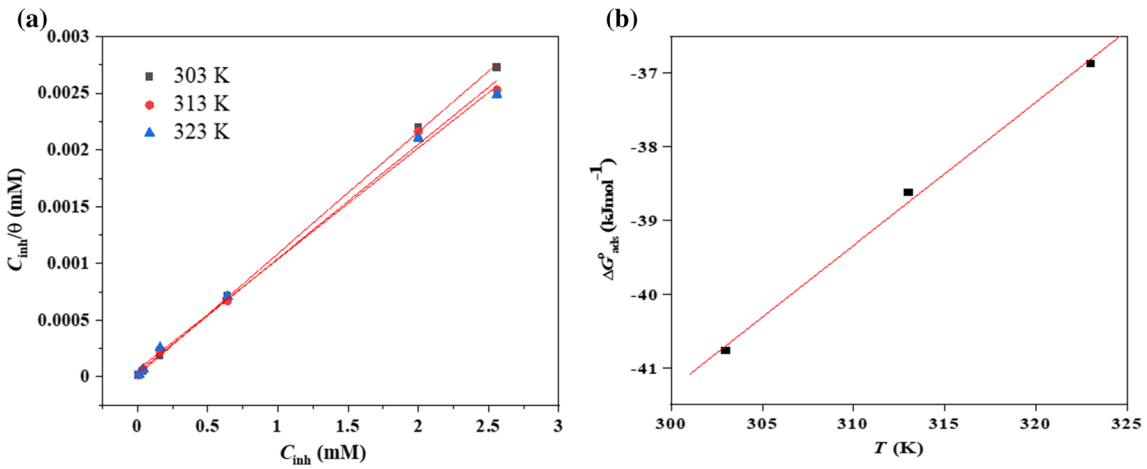

Fig. 5 **a** Langmuir isotherm plot and **b** ΔG°_{ads} Vs. T plot for MBS adsorption on AA6061in 0.5 M HCl

Table 4 The adsorption parameters for MBS

Temp. (K)	K_{ads} (Lmol^{-1})	slope	R^2	ΔG_{ads} (kJmol^{-1})	ΔH_{ads} (kJmol^{-1})	ΔS_{ads} (kJmol^{-1}K^{-1})
303	70,549.72	1.0728	0.9998	− 40.76		
313	27,342.35	1.0070	0.9982	− 38.62	− 99.72	− 0.1948
323	16,537.37	0.9787	0.9983	− 36.87		

$\Delta G^{\circ}ads$ values indicated the spontaneous adsorption of MBS on the alloy's surface.

In exothermic adsorption ($\Delta H^{\circ}_{ads} < 0$), the adsorption type may be physisorption, chemisorption, or mixed-type. As per the literature, ΔH°_{ads} value for physisorption is lower than −41.86 kJmol^{-1}, and for chemisorption, it must approach −100 kJmol^{-1} [43]. The estimated value of ΔH°_{ads} in the present work (Table 4) is −99.72 kJmol^{-1}, almost closer to −100 kJmol^{-1}. It indicates that MBS molecules preferably undergo chemisorption on the alloy surface. It is also supported by the fact that IE of MBS increased with rising temperature, particularly above 2 mM concentration of MBS, as explained earlier. The value of ΔS°_{ads} is negative, which indicates that inhibition results in a decrease in disorder [44].

3.2.5 Mechanism of Inhibition for AA6061 Corrosion

The following mechanism for Al corrosion in the hydrochloric acid media has been suggested [45].

At anode,

$$Al + Cl^{-} \leftrightarrows AlCl^{-}_{ads} \quad (14)$$

$$AlCl^{-}_{ads} + Cl^{-} \rightarrow AlCl^{+}_{2} + 3e^{-} \quad (15)$$

At cathode,

$$H^{+} + e^{-} \rightarrow H_{ads} \quad (16)$$

$$H_{ads} + H_{ads} \rightarrow H_2 \quad (17)$$

Most of the organic compounds prevent metals/alloy corrosion by surface adsorption. It can be possible through physisorption, chemisorption, or both types of adsorption of inhibitor molecules. As explained earlier, it is evident that MBS controls the deterioration of AA6061 in 0.5 HCl through a mixed adsorption mechanism based on the values of ΔG^{o}_{ads}.

The alloy surface acquires a positive charge in an acidic environment because the pH_{ZCh} value (i.e., the pH value corresponding to zero charge potential) for Al is 9.1. Hence, the chloride ions with a negative charge are adsorbed first on the positively charged alloy surface by the electrostatic forces of attraction (Fig. 6). MBS can easily protonate at the amine nitrogen in the acidic medium, and the protonated species formed, $[MBS\text{-}H_x]^{x+}$, can electrostatically adsorb on the negatively charged alloy leading to physisorption (Fig. 6). In the neutral MBS molecules (Enol/Keto form), π-orbitals of the benzene ring and lone pair electrons of nitrogen/oxygen atoms can lead to coordinate bond formation [46]. It consists of the donation of electrons into the vacant p-orbitals of aluminum. This bond formation is responsible for the observed chemisorption (Fig. 6). The presence of heteroatoms (N, O), aromatic ring, and electron-releasing groups (–NH_2 and –OH) in the MBS molecule are responsible for its stronger adsorption and higher inhibition activity.

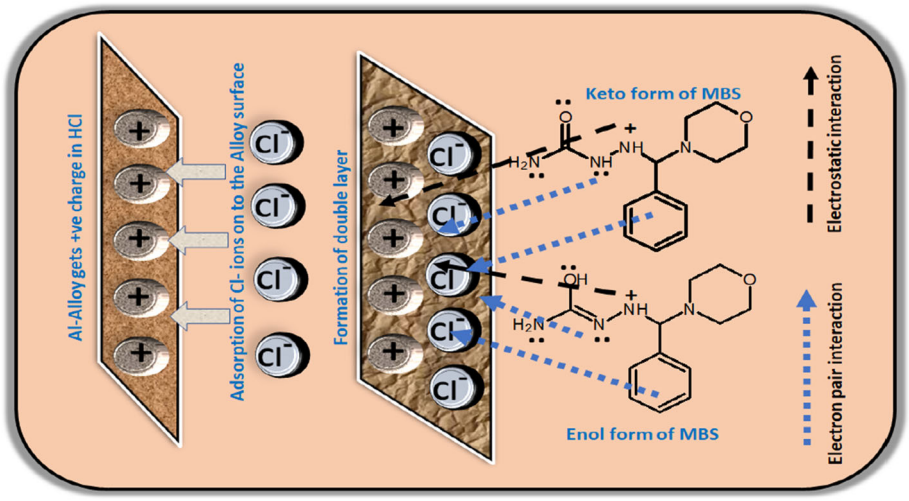

Fig. 6 Schematic illustration for corrosion inhibition mechanism of MBS

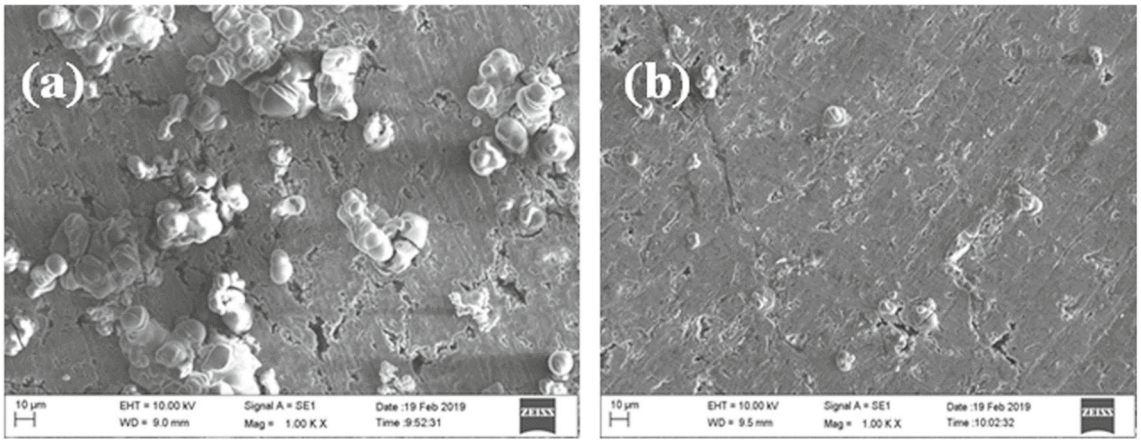

Fig. 7 SEM images of AA6061 specimen dipped in **a** 0.5 M HCl and **b** (0.5 M HCl + 2.56 mM MBS)

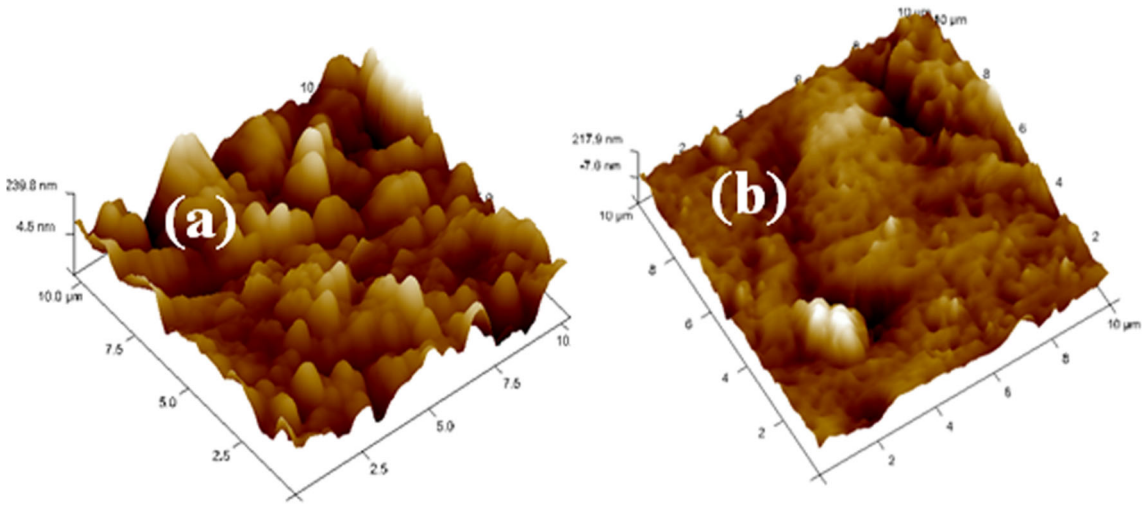

Fig. 8 AFM images of AA6061 specimen dipped in **a** 0.5 M HCl and **b** (0.5 M HCl + 2.56 mM MBS)

Table 5 AFM data for AA6061 specimen dipped in 0.5 M HCl and (0.5 M HCl + 2.56 mM MBS)

Specimen	Medium	R_a	R_q
AA6061 alloy	0.5 M HCl	88.3	114
	0.5 M HCl + 2.56 mM MBS	47.9	51.6

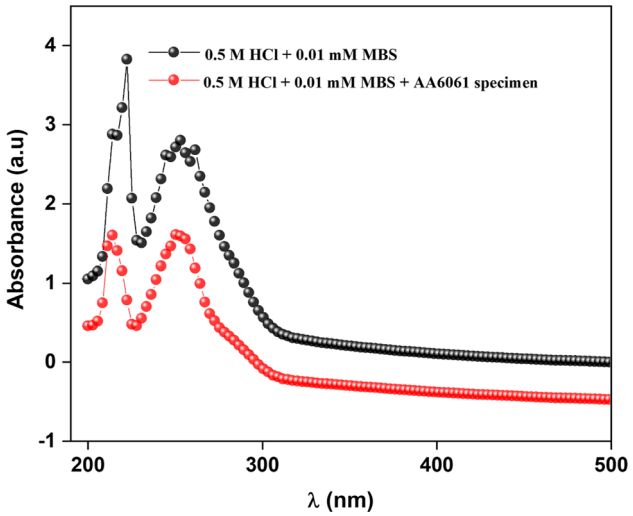

Fig. 9 Absorption spectra of 0.01 mM MBS in 0.5 M HCl before and after immersion of AA6061 coupon

3.2.6 Surface morphology Studies

SEM images of AA6061 specimen immersed in the blank (0.5MHCl) and inhibited medium (0.5 M HCl + 2.56 mM MBS) are given in Fig. 7 a and b. In 0.5 M HCl, the alloy surface was damaged, and many pits can be seen on the surface due to the acid's strong corrosive activity. However, the specimen exposed to the inhibited medium (Fig. 7b) showed fewer pits and reduced surface roughness. It may be due to the MBS adsorption on the alloy's surface, forming a protective film.

The atomic force microscopy images of AA6061 specimen immersed in the blank (0.5 M HCl) and inhibited solutions (0.5 M HCl + 2.56 mM MBS) have displayed in Fig. 8a and b, respectively. Table 5 displays the average surface roughness (R_a) and root mean square roughness (R_q) values of the corroded and inhibited alloy specimen. It is evident from these results that the inhibited alloy specimen's surface roughness was drastically reduced compared to that of the corroded alloy specimen. Thus, the reduced roughness of the inhibited specimen surface is due to the adsorption of MBS on the alloy. As a consequence, the AA6061 is secured against corrosion.

3.2.7 Analysis of UV–Visible Absorption Spectra

UV-Visible spectra can be a helpful tool to confirm the adsorption of MBS on the alloy surface. The UV-Vis spectra of 0.01 mM MBS in a 0.5 M HCl recorded at room temperature showed two absorption peaks at 226 and 256 nm (Fig. 9), corresponding to $\pi \rightarrow \pi^*$ and $n \rightarrow \pi^*$ transition, respectively. Further, AA6061 alloy was immersed in the 0.5 M HCl solution containing 0.01 mM MBS for one h, and the medium's UV-Vis spectra were recorded. This time the spectra retained the same two peaks but with reduced intensity. The reduction in intensity supports the adsorption of MBS on the alloy surface.

3.2.8 Theoretical Studies

To understand the structure–activity relation between the inhibitor (MBS) and its inhibition efficiency, quantum chem-

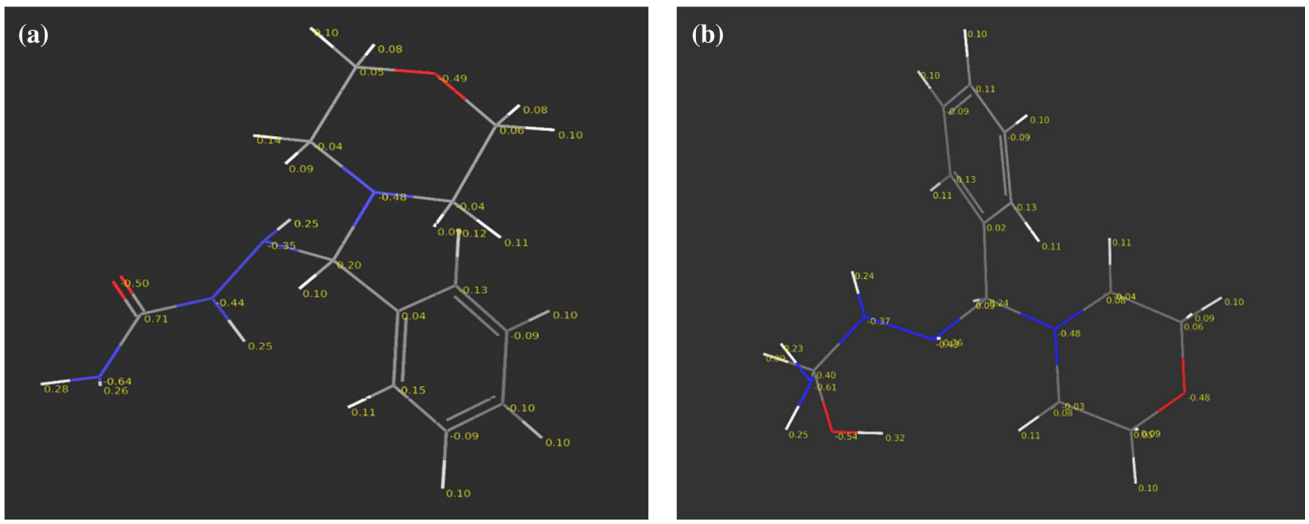

Fig. 10 Mullikan charges on atoms **a** Keto and **b** Enol form of MBS

Table 6 Mullikan charges on atoms in Keto and enol form of MBS molecule

Atoms	Mullikan charges on MBS	
	Keto form	Enol form
C9	− 0.0379	− 0.0417
C13	− 0.0422	− 0.0327
C14	− 0.1508	− 0.1315
C15	− 0.0887	− 0.0895
C16	− 0.1047	− 0.1074
C17	− 0.0876	− 0.0882
C18	− 0.1274	− 0.1263
N2	− 0.4361	− 0.3656
N3	− 0.6355	− 0.6092
N5	− 0.3513	− 0.4289
N7	− 0.4751	− 0.4752
O11	− 0.4862	− 0.4839
C1	0.0712	0.3972
C6	0.1968	0.2403
C8	0.0367	0.0216
C10	0.0515	0.0557
C12	0.0596	0.0530
O4	− 0.4998	− 0.5401

ical calculations have been performed. The electron-donating tendency of an organic molecule and its interaction with the metal surface is the primary reason for the corrosion inhibition property. The effect of these parameters on the inhibition efficiency has been proved with DFT calculations. The MBS frontier molecular orbital energies (E_{HOMO} and E_{LUMO}), energy gap (E_g), and Mullikan charges on atoms were obtained. Mullikan charges detect the desirable adsorption sites on the inhibitor molecule and establish an electron donor–acceptor relation between the inhibitor molecule–metal surface. In this case, the MBS inhibitor exhibits keto–enol tautomerism. Figure 10a and b shows the Mullikan charges on atoms in keto and enol form of MBS molecule. Heteroatoms in MBS with more negative Mullikan charges (Table 6) are considered favorable candidates for the donor–acceptor property. A higher negative charge was found in the keto form on the oxygen of C=O (− 0.50) and nitrogen of NH_2 (− 0.64) group. For MBS's enol form, a higher negative charge was found on the oxygen of OH (− 0.54) and nitrogen of NH_2 (− 0.61) group. These higher negative charge centers act as adsorption sites on the MBS molecule leading to its stronger adsorption, which resists the corrosion of AA6061 alloy. The optimized structures of keto and enol form of MBS inhibitor and their HOMO and LUMO orbitals are shown in Fig. 11.

The quantum chemical parameters have been computed using the following relations [47, 48].

E_{HOMO} is related to I, whereas E_{LUMO} to A, as follows:

$$I = -E_{\mathrm{HOMO}} \tag{18}$$

$$A = -E_{\mathrm{LUMO}} \tag{19}$$

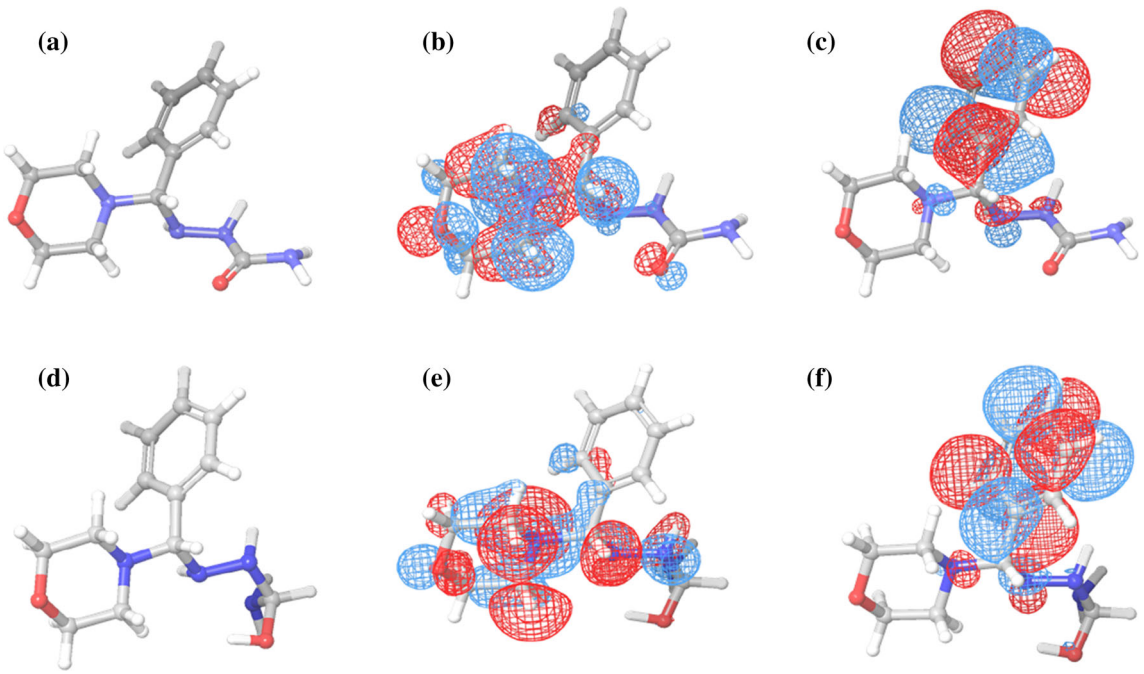

Fig. 11 **a** Optimized structure, **b** HOMO, and **c** LUMO of Keto form of MBS; **d** Optimized structure, **e** HOMO, and **f** LUMO of Enol form of MBS

Table 7 DFT parameters for Keto and Enol form of MBS

Property of MBS	Keto form	Enol form
E_{HOMO}	− 5.9938 eV	− 6.0597 eV
E_{LUMO}	− 0.4128 eV	− 0.2892 eV
Bandgap (E_g)	5.5810 eV	5.7705 eV
Ionization potential (I)	5.9938 eV	6.0597 eV
Electron affinity (A)	0.4128 eV	0.2892 eV
Electronegativity (χ)	3.2033 eV	3.1744 eV
Global hardness (η)	2.7905 eV	2.8852 eV
Global softness (σ)	0.3583	0.3466
Fraction of electron transferred (ΔN)	0.1929	0.1916

The electronegativity (χ) and the hardness (η) values have been obtained using Eg. (20) and (21), respectively.

$$\chi = \frac{I + A}{2} \tag{20}$$

$$\eta = \frac{I - A}{2} \tag{21}$$

The number of electrons transferred (ΔN) has computed from Eg. (22):

$$\Delta N = \frac{\chi_{Al} - \chi_{MBS}}{2(\eta_{Al} + \eta_{MBS})} \tag{22}$$

where χ_{Al} and χ_{MBS} indicate the electronegativity of Al and MBS, respectively, while η_{Al} and η_{MBS} represent the hardness of Al and MBS, respectively.

The softness value was obtained as per the relation,

$$\sigma = \frac{1}{\eta} \tag{23}$$

The various quantum parameters obtained from DFT for the keto and enol form of MBS are listed in Table 7.

Generally, the corrosion process takes place via the physical or chemical adsorption of inhibitor molecules. Physical adsorption involves the electrostatic interaction of charged metal surface and charged inhibitor species in the medium. Chemical adsorption occurs by the transfer of electrons from the inhibitor molecule to the vacant orbitals of the metal with low energy. The ΔG°_{ads} values (Table 4) indicated the mixed adsorption of MBS molecules. The increase in IE with temperature (Table 1) and the ΔH°_{ads} values (Table 4) suggests that MBS significantly underwent chemisorption. The reactivity shown by the inhibitor can be suitably related to its E_{HOMO} and E_{LUMO} values. It is clear from Fig. 11 a–f that the density distribution on HOMO and LUMO in keto and enol forms of MBS are similar. The density distributions on HOMO focused around the morpholine ring. However, the LUMO's density distributions were mainly around the benzene ring. As reported earlier, inhibitor with higher E_{HOMO} values shows a greater tendency to donate electrons to the metal, whereas a higher E_{LUMO} value accepts electrons from the metal [49]. MBS's keto form showed a higher E_{HOMO} and lower E_{LUMO} value (Table 7) than the enol form. It reveals that MBS's keto form can donate electrons to the Al metal, and the enol form accepts electrons from Al metal. Thus, the unoccupied *d*-orbital of the Al atom can accept electrons from the keto form of MBS, leading to a coordinate bond. In addition, the enol form of MBS can take electrons from the Al atom with its antibonding orbitals to form a back-donating bond.

It is clear from Mullikan charges on atoms of keto and enol form of MBS (Table 6) that nitrogen and oxygen atoms are the probable active sites for MBS adsorption on the Al-alloy surface. In the present work, Fukui indices values for MBS are not given because the other quantum chemical parameters calculated have provided conclusive results on MBS inhibition activity. The parameters such as global hardness and softness give information on the reactivity of inhibitor molecules. A molecule with a low *Eg* value is more polarizable and exhibits high chemical reactivity and low kinetic stability, and is said to be a soft molecule [50]. As reported, inhibitor molecules with the highest global softness and lowest global hardness provide better adsorption onto a metallic surface [51]. Hence, keto MBS with a lower *Eg* value, higher softness, and lower hardness than enol MBS were expected to show better reactivity and adsorption onto the Al-alloy surface (Table 7).

3.2.9 Comparison of Inhibition Performance with Other Reported Inhibitors for AA6061

The inhibition efficiency of MBS has been compared with other reported corrosion inhibitors of AA6061 in HCl medium. It is clear from Table 8 that the inhibitor used in the present work, MBS, has shown the highest inhibition efficiency compared to other reported ones.

4 Conclusion

- MBS behaves as an effective acid corrosion inhibitor of AA6061 alloy.
- The inhibition efficiency of MBS was found to improve with its concentration.
- Inhibition efficiency has declined with an increase in temperature up to 0.64 mM concentration of MBS. However, it has been improved with a rise in temperature in the presence of 2 and 2.56 mM MBS.
- The maximum efficiency of 98.92% was observed by the EIS method at 2.56 mM MBS and 323 K.
- MBS was an inhibitor of mixed-type.

Table 8 A comparison of inhibition performance of MBS with other reported inhibitors

Inhibitors	Medium (Inh. Conc. and temp.)	Maximum IE (%)			Remarks, if any	References
		WL	PDP	EIS		
N, N'-bis (Salicylidene)-1, 4-Diaminophenelyne	1 M HCl (at 500 ppm and 303 K)	87	–	–	IE decreases with rise in temperature (303 K)	[52]
N, N'-bis (3-Methoxy Salicylidene)-1, 4 Diamino phenelyne	1 M HCl (at 500 ppm and 303 K)	94	–	–		
N, N'-bis (Salicylidene)-1, 4-Diaminobutane	1 M HCl (at 100 ppm & 303 K)	75	74.2	73.9	IE decreases with increase in temp (303–323 K)	[53]
N, N'-bis (3-Methoxy Salicylidene)-1, 4 Diaminobutane	1 M HCl (at 100 ppm & 303 K)	79	78.6	78.1		
Starch	0.1 M HCl (at 800 ppm and 323 K)	–	63.44	62.89	IE increases with increase in temp (303–323 K)	[23]
Dextran	1 M HCl (at 0.4 g L^{-1} & 303 K)	–	74.6	77.9	IE decreases with increase in temp (303–323 K)	[54]
Ethyl-2-amino-4-methyl-1,3-thiazole-5-carboxylate	0.05 M HCl (at 100 ppm and 333 K)	92.74	92.56	92.77	IE increases with increase in temp (303–333 K)	[55]
5-(3-Pryridyl)-4H-1,2,4-triazole-3-thiol	0.1 M HCl (at 40 ppm and 333 K)	91.9	94.2	94.1	IE increases with increase in temp (303–333 K)	[56]
1-butyl-3- methylimidazolium thiocyanate	1 M HCl (at 4 mM and 303 K)	98.2	98.0	98.4	IE decreases with increase in temp (303–363 K)	[57]
Glutathione (reduced)	0.5 M HCl (at 0.7 mM and 303 K)	87.8	88.9	–	IE decreases with increase in temp (303–333 K)	[33]
Cysteine	0.5 M HCl (at 0.7 mM and 303 K)	–	74.6	72.18	IE decreases with increase in temp (303–333 K)	[58]
MBS	0.5 M HCl (at 2.56 mM and 323 K)	–	96.42	98.92	IE increases with increase in temp (303–323 K)	Present work

- MBS adsorption on the alloy surface occurred by both physisorption and chemisorption. Adsorption isotherm has obeyed the Langmuir isotherm model.
- The theoretical method by DFT validated the good inhibition performance evinced by MBS through electrochemical methods

Acknowledgements Ms. Maithili K gratefully acknowledged the Manipal Institute of Technology, Manipal Academy of Higher Education, Manipal, for extending the laboratory facilities.

Funding Open access funding provided by Manipal Academy of Higher Education, Manipal.

References

1. Miller, W.S.; Zhuang, L.; Bottema, J.; Wittebrood, A.J.; De Smet, P.; Haszier, A.; Vieregge, A.: Recent development in aluminium alloys for the automotive industry. Mater. Sci. Eng. A **280**, 37–49 (2000). https://doi.org/10.1016/S0921-5093(99)00653-X
2. Mukhopadhyay, P.: Alloy designation, processing, and use of AA6XXX series aluminium alloys. ISRN Metall. **2012**, 165082 (2012). https://doi.org/10.5402/2012/165082
3. Davis, J.R.: Corrosion of aluminium and aluminium alloys. ASM International, Ohio (1999). https://doi.org/10.31399/asm.tb.caaa.9781627082990
4. Raja, P.B.; Ismail, M.; Ghoreishiamiri, S.; Mirza, J.; Ismail, M.C.; Kakooei, S.; Rahim, A.A.: Reviews on corrosion inhibitors–a short view. Chem. Eng. Commun. **203**, 1145–1156 (2016). https://doi.org/10.1080/00986445.2016.1172485
5. Rosenfeld, I.L.: Corrosion Inhibitors. McGraw Hill, New York (1981)
6. Xhanari, K.; Finsgar, M.: Organic corrosion inhibitors for aluminium and its alloys in acid solutions: a review. RSC Adv. **6**, 62833–62857 (2016). https://doi.org/10.1039/c6ra11818f
7. Xhanari, K.; Finsgar, M.: The corrosion inhibition of AA6082 aluminium alloy by certain azoles in chloride solution: Electro-

chemistry and surface analysis. Coat. **9**, 380 (2019). https://doi.org/10.3390/coatings9060380
8. Shetty, P.: Schiff bases: an overview of their corrosion inhibition activity in acid media against mild steel. Chem. Eng. Commun. **207**, 985–1029 (2020). https://doi.org/10.1080/00986445.2019.1630387
9. Bala, S.; Sharma, N.; Kajal, A.; Kamboj, S.; Saini, V.: Mannich Bases: An important pharmacophore in present scenario. Inter. J. Med. Chem. **2014**, 191072 (2014). https://doi.org/10.1155/2014/191072
10. Quraishi, M.A.; Ahamad, I.; Singh, A.K.; Shukla, S.K.; Lal, B.; Singh, V.: N- (Piperidinomethyl)-3-[(pyridylidene)amino]isatin: a new and effective acid corrosion inhibitor for mild steel. Mater. Chem. Phys. **112**, 1035–1039 (2008). https://doi.org/10.1016/j.matchemphys.2008.07.011
11. Ahamad, I.; Prasad, R.; Quraishi, M.A.: Adsorption and inhibitive properties of some new Mannich base of isatin derivatives on corrosion of mild steel in acidic media. Corros. Sci. **52**, 1472–1481 (2010). https://doi.org/10.1016/j.corsci.2010.01.015
12. Singh, A.K.; Quraishi, M.A.: Inhibiting effects of 5-substituted isatin-based Mannich bases on the corrosion of mild steel in hydrochloric acid solution. J. Appl. Electrochem. **40**, 1293–1306 (2010). https://doi.org/10.1007/s10800-010-0079-9
13. Jeeva, M.; Prabhu, G.V.; Rajesh, C.M.: Inhibition effect of nicotinamide and its Mannich base derivatives on mild steel corrosion in HCl. J. Mater. Sci. **52**, 12861–12888 (2017). https://doi.org/10.1007/s10853-017-1401-2
14. Lavanya, D.K.; Priya, F.V.; Vijaya, D.P.: Green approach to corrosion inhibition of mild steel in hydrochloric acid by 1-[morpholin-4-yl(thiophen-2-yl) methyl] thiourea. J. Fail. Anal. Prev. **20**, 494–502 (2020). https://doi.org/10.1007/s11668-020-00850-9
15. Viswanathan, M.: Synthesis, spectral, X-ray diffraction and antibacterial studies of oxovanadium (IV) and dioxouranium(VI) complexes of N-(1-mopholinobenzyl) semicarbazide. Asian J. Chem. **28**, 1621–1623 (2016). https://doi.org/10.14233/ajchem.2016.19786
16. Fontana, M.G.: Corrosion engineering. McGraw-Hill, New York (1987)
17. Bentiss, F.; Lebrini, M.; Lagrenee, M.: Thermodynamic characterization of metal dissolution and inhibitor adsorption processes in mild steel/2,5- bis (n-thienyl)-1,3,4-thiadiazoles/hydrochloric acid system. Corros. Sci. **47**, 2915–2931 (2005). https://doi.org/10.1016/j.corsci.2005.05.034
18. Charitha, B.P.; Rao, P.: Pollulan as a potent green inhibitor for corrosion mitigation of aluminium composite: electrochemical and surface studies. Int. J. Biol. Macromol. **112**, 461–472 (2018). https://doi.org/10.1016/j.ijbiomac.2018.01.218
19. Abboud, Y.; Abourriche, A.; Saffaj Berrada, T.M.; Charrouf, M.; Bennamara, A.; Cherqaoui, A.; Takky, D.: The inhibition of mild steel corrosion in acidic medium by 2,2′-bis(benzimidazole). Appl. Surf. Sci. **252**, 8178–8184 (2006). https://doi.org/10.1016/j.apsusc.2005.10.060
20. Zhang, Q.; Hua, Y.: Corrosion inhibition of aluminium in hydrochloric acid solution by alkyl imidazolium ionic liquids. Mater. Chem. Phys. **119**, 57–64 (2010). https://doi.org/10.1016/j.matchemphys.2009.07.035
21. Li, W.; He, Q.; Zhang, S.; Pel, C.; Hou, B.: Some new triazole derivatives as inhibitors for mild steel corrosion in acidic medium. J. Appl. Electrochem. **38**, 289–295 (2008). https://doi.org/10.1007/s10800-007-9437-7
22. Lenderink, H.J.W.; Linden, M.V.D.; De Wit, J.H.W.: Corrosion of aluminium in acidic and neutral solutions. Electrochim. Acta **38**, 1989–1992 (1993). https://doi.org/10.1016/0013-4686(93)80329-X
23. Charitha, B.P.; Rao, P.: Starch as an ecofriendly green inhibitor for corrosion control of 6061-Al alloy. J. Mater. Environ. Sci. **8**, 78–89 (2017)
24. Metikos-Hukovic, M.; Babic, R.: Corrosion protection of aluminium in acidic chloride solutions with nontoxic inhibitors. J. Appl. Electrochem. **28**, 433–439 (1998)
25. Metikos-Hukovic, M.; Babic, R.; Grubac, Z.: The study of aluminium corrosion in acidic solution with nontoxic inhibitors. J. Appl. Electrochem. **32**, 35–41 (2002)
26. Macdonald, J.R.: Impedance Spectroscopy. Ann. Biomed. Eng. **20**, 289–305 (1992). https://doi.org/10.1007/BF02368532
27. Hsu, C.H.; Mansfeld, F.: Concerning the conversion of the constant phase element parameter Y_0 into a capacitance. Corros. **57**, 747–748 (2001). https://doi.org/10.5006/1.3280607
28. Mansfeld, F.; Lin, S.; Kim, S.; Shih, H.: Electrochemical impedance spectroscopy as a monitoring tool for passivation and localized corrosion of aluminium alloys. Mater. Corros. **39**, 487–492 (1988). https://doi.org/10.1002/maco.19880391102
29. Brett, C.M.A.: On the electrochemical behavior of aluminium in acidic chloride solution. Corros. Sci. **33**, 203–210 (1992)
30. Abd El Rehim, S.S.; Hassan, H.H.; Amin, M.A.: Corrosion inhibition of aluminium by 1, 1(lauryl amido)propyl ammonium chloride in HCl solution. Mater. Chem. Phys. **70**, 64–72 (2001). https://doi.org/10.1016/S0254-0584(00)00468-5
31. Umoren, S.A.; Li, Y.; Wang, F.H.: Effect of polyacrylic acid on the corrosion behaviour of aluminium in sulphuric acid solution. J. Solid State Electrochem. **14**, 2293–2305 (2010). https://doi.org/10.1007/s10008-010-1064-2
32. Bessone, J.B.; Salinas, D.R.; Mayer, C.; Ebert, M.; Lorenz, W.J.: An EIS study of aluminium barrier-type oxide films formed in different media. Electrochim. Acta **37**, 2283–2290 (1992). https://doi.org/10.1016/0013-4686(92)85124-4
33. Nagalaxmi; Shetty, P.; Kumari, P.P.: Inhibitive action of glutathione reduced on the deterioration of AA6061 in 0.5M HCl. Tribol. Ind. **42**, 214–224 (2020). https://doi.org/10.24874/ti.785.10.19.02
34. Schorr, M.; Yahalom, J.: The significance of the energy of activation for the dissolution reaction of metal in acids. Corros. Sci. **12**, 867–868 (1972)
35. Abdel Rehim, S.S.; Ibrahim, M.A.M.; Khaled, K.F.: 4-Aminoantipyrine as an inhibitor of mild steel corrosion in HCl solution. J. Appl. Electrochem. **29**, 593–599 (1999). https://doi.org/10.1023/A:1003450818083
36. Osman, M.M.; El-Ghazawy, R.A.; Al-Sabagh, A.M.: Corrosion inhibitor of some surfactants derived from maleic–oleic acid adduct on mild steel in 1 M H_2SO_4. Mater. Chem. Phys. **80**, 55–62 (2003). https://doi.org/10.1016/S0254-0584(01)00588-0
37. Mansfeld, F.: Corrosion mechanisms. Marcel Dekkar Inc, New York (1987)
38. Singh, A.K.; Quraishi, M.A.: Investigation of the effect of disulfiram on corrosion of mild steel in hydrochloric acid solution. Corros. Sci. **53**, 1288–1297 (2011). https://doi.org/10.1016/j.corsci.2011.01.002
39. Atta, N.F.; Fekry, A.M.; Hassaneen, H.M.: Corrosion inhibition, hydrogen evolution and antibacterial properties of newly synthesized organic inhibitors on 316L stainless steel alloy in acid medium. Int. J. Hydrog. Energy **36**, 6462–6471 (2011). https://doi.org/10.1016/j.ijhydene.2011.02.134
40. Bayol, E.; Kayakırılmaz, K.; Erbil, M.: The inhibitive effect of hexamethylenetetramine on the acid corrosion of steel. Mater. Chem. Phys. **104**, 74–82 (2007). https://doi.org/10.1016/j.matchemphys.2007.02.073
41. Rosliza, R.; Noraaini, A.; Wan Nik, W.B.: Study on the effect of vanillin on the corrosion inhibition of aluminium alloy. J. Appl. Electrochem. **40**, 833–840 (2010). https://doi.org/10.1007/s10800-009-0066-1

42. Tang, L.; Li, X.; Li, L.; Mu, G.; Liu, G.: Interfacial behavior of 4-(2-pyridylazo) resorcin between steel and hydrochloric acid. Surf. Coat. Technol. **201**, 384–388 (2006). https://doi.org/10.1016/j.surfcoat.2005.11.132
43. Ahamad, I.; Prasad, R.; Quraishi, M.A.: Thermodynamic, electrochemical and quantum chemical investigation of some Schiff bases as corrosion inhibitors for mild steel in hydrochloric acid solutions. Corros. Sci. **52**, 933–942 (2010). https://doi.org/10.1016/j.corsci.2009.11.016
44. Kumari, P.P.; Shetty, P.; Rao, A.S.; Sunil, D.: Corrosion inhibition and adsorption behaviour of (2E)-2-(3-hydroxy-2-methoxybenzylidene) hydrazinecarbothiamide on mild steel in 1M HCl. Rev. Roum. Chim. **59**, 323–333 (2014)
45. El-Awady, A.A.; Abd-El-Nabey, B.A.; Aziz, S.G.: Thermodynamic and kinetic factors in chloride ion pitting and nitrogen donor ligand inhibition of aluminium metal corrosion in aggressive acid media. J. Chem. Soc. Faraday Trans. **89**, 795–802 (1993). https://doi.org/10.1039/FT9938900795
46. Trabanelli, G.; Carassiti, V.: Mechanism and phenomenology of organic inhibitors. In: Fontana, M.G.; Staehle, R.W. (Eds.) Advances in Corrosion Science and Technology, pp. 147–228. Plenum Press, New York (1976)
47. Pearson, R.G.: Absolute electronegativity and hardness: Application to inorganic chemistry. Inorg. Chem. **27**, 734–740 (1988)
48. Chang-Guo, Z.; Nichols, J.A.; Dixon, D.A.: Ionization potential, electron affinity, electronegativity, hardness, and electron excitation energy: molecular properties from density functional theory orbital energies. J. Phys. Chem. A **107**, 4184–4195 (2003). https://doi.org/10.1021/jp0225774
49. Azooz, R.E.: EDTA as a corrosion inhibitor for Al in 05 M HCl: adsorption, thermodynamic and theoretical study. J. Electrochem. Sci. Eng. **6**, 235–251 (2016). https://doi.org/10.5599/jese.300
50. Madkour, L.H.; Elroby, S.K.: Inhibitive properties, thermodynamic, kinetics, and quantum chemical calculations of polydentate Schiff base compounds as corrosion inhibitors for iron in acidic and alkaline media. Int. J. Indus. Chem. **6**, 165–184 (2015). https://doi.org/10.1007/s40090-015-0039-7
51. Islam, N.; Ghosh, D.C.: A new algorithm for the evaluation of the global hardness of polyatomic molecules. Mol. Phys. **109**, 917–931 (2011). https://doi.org/10.1080/00268976.2011.558856
52. Fakrudeen, S.P.; Bheema Raju, V.: Electrochemical behaviour of AA6061 alloy in 1M hydrochloric acid using Schiff base compounds as corrosion inhibitors. J. Mater. Environ. Sci. **4**, 326–337 (2013)
53. Fakrudeen, S.P.; Ananda Murthy, H.C.; Bheema Raju, V.: Corrosion inhibition of AA6061 and AA6063 alloy in hydrochloric acid media by Schiff base compounds. J. Chil. Chem. Soc. **57**, 1364–1371 (2012)
54. Charitha, B.P.; Rao, P.: Electrochemical and adsorption studies for the corrosion control of 6061 Al alloy using eco-friendly inhibitor. Surf. Eng. Appl. Electrochem. **53**, 551–559 (2017). https://doi.org/10.3103/S1068375517060035
55. Raviprabha, K.; Bhat, R.S.: Inhibition effects of ethyl-2-amino-4-methyl-1,3-thiazole-5-carboxylate on the corrosion of AA6061 alloy in hydrochloric acid media. J. Fail. Anal. Prev. **19**, 1464–1474 (2019). https://doi.org/10.1007/s11668-019-00744-5
56. Raviprabha, K.; Bhat, R.S.: 5-(3-Pryridyl)-4H-1,2,4-triazole-3-thiol as potential corrosion inhibitor for AA6061 aluminium alloy in 0.1 M hydrochloric acid solution. Surf. Eng. Appl. Electrochem. **55**, 723–733 (2019). https://doi.org/10.3103/S1068375519060103
57. Wang, X.; Huang, A.; Dongquan, L.; Talha, M.; Liu, H.; Yuanhua, L.: Imidazolium-based ionic liquid as efficient corrosion inhibitor for AA 6061 alloy in HCl solution. Mater. **13**, 4672 (2020). https://doi.org/10.3390/ma13204672
58. Kumari, P.P.; Shetty, P.; Nagalaxmi; Sunil, D.: Effect of cysteine as environmentally friendly inhibitor on AA6061-T6 corrosion in 0.5 M HCl Electrochemical and Surface Studies. Surf. Eng. Appl. Electrochem. **56**, 624–634 (2020)